arXiv:1907.05466v1 [physics.atom-ph] 11 Jul 2019

Quantum rotation sensing with dual Sagnac interferometrs in an atom-optical waveguide

E. R. Moan, R. A. Horne,* T. Arpornthip,† Z. Luo, A. J. Fallon, S. J. Berl, and C. A. Sackett‡
Department of Physics, University of Virginia, Charlottesville, Virginia 22904, USA
(Dated: December 2, 2023)

Sensitive and accurate rotation sensing is a critical requirement for applications such as inertial navigation [1], north-finding [2], geophysical analysis [3], and tests of general relativity [4]. One effective technique used for rotation sensing is Sagnac interferometry, in which a wave is split, traverses two paths that enclose an area, and then recombined. The resulting interference signal depends on the rotation rate of the system and the area enclosed by the paths [5]. Optical Sagnac interferometers are an important component in present-day navigation systems [6], but suffer from limited sensitivity and stability. Interferometers using matter waves are intrinsically more sensitive and have demonstrated superior gyroscope performance [7–9], but the benefits have not been large enough to offset the substantial increase in apparatus size and complexity that atomic systems require. It has long been hoped that these problems might be overcome using atoms confined in a guiding potential or trap, as opposed to atoms falling in free space [10–12]. This allows the atoms to be supported against gravity, so a long measurement time can be achieved without requiring a large drop distance. The guiding potential can also be used to control the trajectory of the atoms, causing them to move in a circular loop that provides the optimum enclosed area for a given linear size [13]. Here we use such an approach to demonstrate a rotation measurement with Earth-rate sensitivity.

A small number of trapped-atom Sagnac interferometers have been demonstrated in the past,[14–18] but none have been used to make a quantitative rotation measurement. The largest enclosed areas have been achieved using a linear interferometer that is translated along a direction perpendicular to the interferometer axis,[19] but this approach may not be well-suited for inertial measurements in a moving vehicle. Here, we demonstrate a true two-dimensional interferometer configuration in which atoms travel in circular trajectories through a static confining potential. We obtain an effective enclosed area of 0.50 mm^2, compared to areas of 0.20 mm^2 reported by Wu *et al.*[15] and 0.35 mm^2 recently obtained by the Los Alamos group.[18] Our approach is readily scalable to weaker traps and multiple orbits by the atoms, making larger areas feasible.

Another key advance is the use of dual counter-propagating interferometer measurements. Here, two Sagnac interferometers are implemented at the same time in the same trap, with atoms travelling at opposite velocities over the same paths. This technique was developed for free space interferometers [8], and allows the common-mode rejection of interferometric phases from accelerations, laser noise, background fields, and other effects that can mask the rotation signal. The Sagnac effect itself is differential and can be extracted by comparing the two individual measurements. This technique is likely to be essential for any practical rotation-sensing system, but has not previously been demonstrated in a trapped-atom system.

Our Sagnac interferometer is implemented using a Bose–Einstein condensate (BEC) confined in a three-dimensional trap, with potential energy

$$V(x,y,z) = \frac{1}{2}m\left(\omega_x^2 x^2 + \omega_y^2 y^2 + \omega_z^2 z^2\right), \qquad (1)$$

where m is the atomic mass and the ω_i are the trap frequencies. The coordinates x, y and z represent the principle axes of the trap. The trap is approximately cylindrically symmetric, with $\omega_x \approx \omega_y \equiv \omega$. The condensate is produced nominally at rest in the centre of the trap.

The atoms are manipulated using a set of standing wave Bragg lasers [20–22] propagating along the x and y directions. The beams couple atomic states with momenta $\mathbf{p}$ and $\mathbf{p} \pm 2\hbar\mathbf{k}$, where $\mathbf{k}$ is the wave vector of the laser. We express this in terms of a velocity kick $v_B = 2\hbar k/m$.

The interferometer measurement begins by applying the Bragg beams along y. This generates two wave packets with velocities $\mathbf{v} = \pm v_B\hat{\mathbf{y}}$. The atoms move in the trap, following the ordinary trajectory for a harmonic oscillator $x(t) = 0$ and $y(t) = \pm(v_B/\omega)\sin\omega t$. After a time $t_1 = \pi/(2\omega)$, the atoms come to rest near the classical turning point at a radius $R = v_B/\omega$. The Bragg beams traveling along x are then applied to both packets, providing velocity kicks $\pm v_B\hat{\mathbf{x}}$ and generating a total of four packets. Each of these packets now travels in a circle with radius R, as $x(t) = \pm R\sin\omega t$ and $y(t) = \pm R\cos\omega t$. The atoms propagate for time $t_2 = 2\pi/\omega$, completing one full orbit around the trap. The density of the BEC is about 10^{12} cm^{-3}, low enough that the packets can pass through each other with negligible interactions.

After the orbit, the pairs of packets are overlapped again at their locations prior to the x Bragg pulse. The

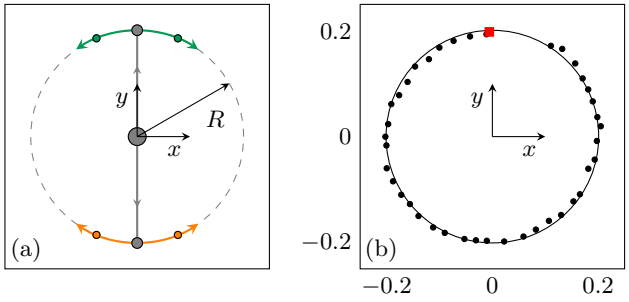


FIG. 1: (a) Trajectories of atoms in the interferometer. The initial condensate (centre) is split into two packets that move along $\pm y$. When the packets reach their turning points at $y = \pm R$, they are split along x, generating four packets that move in circular orbits (green and orange traces). After one complete orbit the packets are recombined, forming two independent interferometers. (b) Experimental data showing the path of one packet, starting at the red square and moving clockwise. The scales are in mm, and the area enclosed by the orbit is 0.13 mm^2.

wave function of a pair can be expressed as

$$|\psi\rangle = \frac{1}{\sqrt{2}}\left(e^{i\Phi/2}|+v_B\rangle + e^{-i\Phi/2}|-v_B\rangle\right), \qquad (2)$$

where Φ is the phase developed between the packets and $|\pm v_B\rangle$ are states with the indicated velocity along x. The x Bragg beams are now applied again. This couples the even superposition $(|+v_B\rangle + |-v_B\rangle)$ back to the zero-momentum state $|0\rangle$, while the odd superposition $(|+v_B\rangle - |-v_B\rangle)$ remains unchanged (up to an overall phase). Projecting the wave function $|\psi\rangle$ onto these superpositions, we find that a fraction $S = \cos^2\Phi/2$ of the atoms are brought back to rest [23, 24].

To detect the result of the recombination, the moving and stationary atoms are allowed to separate, the trap is turned off, and the entire system is observed using absorption imaging in the xy-plane. FIG. 1 shows a schematic of the atomic trajectories and measured positions of one packet as it traverses the trap. A video showing the motion of all four packets is available in the Supplementary Information. FIG. 2(a) shows an absorption image after the recombination pulse.

Note that this sequence produces two independent interferometer measurements. We define Φ_+ as the phase measured for atoms at $y = +R$, and Φ_- as the phase measured at $y = -R$. Each of these individual phases is sensitive to a variety of effects including magnetic field variations, mechanical vibration, and laser phase noise. Most of these effects will be the same for both interferometers, but if the system is rotating with angular velocity $\mathbf{\Omega}$, then the Sagnac phases

$$\Phi_S = \frac{1}{\hbar}\oint \Delta\mathbf{L}\cdot\mathbf{\Omega}\,dt = \frac{4m\Omega A}{\hbar} \qquad (3)$$

will have the opposite sign. Here $\Delta\mathbf{L} = \mathbf{r}_2\times\mathbf{p}_2 - \mathbf{r}_1\times\mathbf{p}_1$ is the difference in angular momentum between the two packets, and $A = \pi R^2$ is the area of a single packet's orbit. This leads to a differential phase

$$\Delta\Phi = \Phi_+ - \Phi_- = 2\Phi_S = \frac{8m\Omega A}{\hbar}. \qquad (4)$$

We implement the interferometer using about 10^4 ^{87}Rb atoms, magnetically trapped in the $F = 2, m_F = 2$ ground state. The apparatus for BEC production and generating the magnetic trap has been previously described [25]. Our time-orbiting potential (TOP) trap [26] uses a special field configuration that allows precise experimental control of the trap parameters. The bias field of the TOP trap rotates as

$$\mathbf{B}_{\rm bias} = B_0\Big[(1+\alpha)\sin(\Omega_1 t)\cos(\Omega_2 t+\beta)\,\hat{\mathbf{x}} + (1-\alpha)\sin(\Omega_1 t)\sin(\Omega_2 t-\beta)\,\hat{\mathbf{y}} + \cos(\Omega_1 t)\,\hat{\mathbf{z}}\Big], \qquad (5)$$

with $\Omega_1 \approx 2\pi\times 10^4$ Hz and $\Omega_2 \approx 2\pi\times 10^3$ Hz. The amplitude asymmetry α and the phase β are nominally zero, but can be adjusted to optimise the trap. The coordinates (x, y, z) are now determined by the coil geometry, with z near vertical. The trap also uses an oscillating quadrupole field,

$$\mathbf{B}_{\rm quad} = \frac{1}{2}B_1'\cos(\Omega_1 t)\big(x\,\hat{\mathbf{x}} + y\,\hat{\mathbf{y}} - 2z\,\hat{\mathbf{z}}\big). \qquad (6)$$

These fields provide a trap potential $V(\mathbf{r}) = \mu_B\langle|\mathbf{B}|\rangle$, where μ_B is the Bohr magneton and $\langle|\mathbf{B}|\rangle$ is the time average of the magnetic field magnitude. Evaluation to second order in the coordinates gives

$$V = -\frac{1}{2}\mu_B B_1 z + \frac{1}{2}m\omega_0^2\left[\left(1+\frac{2\alpha}{7}\right)x^2 + \left(1-\frac{2\alpha}{7}\right)y^2 + \frac{4}{7}\beta xy + \frac{8}{7}z^2\right], \qquad (7)$$

with $\omega_0 = (7\mu_B B_1'^2/64mB_0)^{1/2}$. We set $B_1' = 2mg/\mu_B \approx 31$ G/cm to cancel gravity at the centre of the trap, and with $B_0 \approx 2$ G we obtain $\omega_0 \approx 2\pi\times 9$ Hz.

The actual potential experienced by the atoms varies from (7) due to environmental fields and other experimental imperfections. If this alters the wave packet trajectories so that they fail to overlap after an orbit, then the interferometer will be spoiled. A classical trajectory calculation indicates that the difference in trap frequencies $|\omega_x - \omega_y|/2\pi$ must be less than 0.1 Hz, and the Bragg laser beams must be aligned to better than 10 mrad accuracy. We achieve these requirements by observing the packet trajectories and adjusting α, β, the Bragg beam angles, and the propagation times t_1 and t_2 until both interferometers are closed and interference is observed. The resulting orbits are nearly circular with a radius

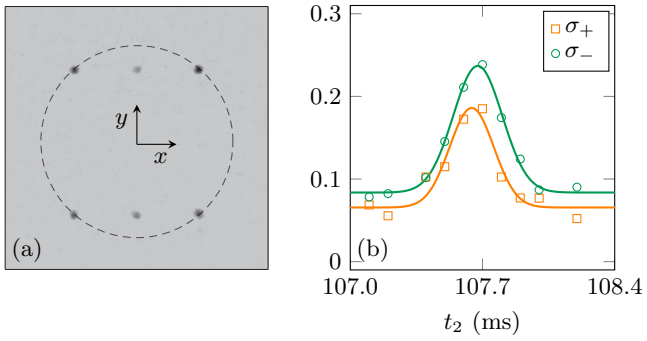


FIG. 2: (a) An absorption image in the xy-plane taken 12 ms after the recombination pulse was applied. Atoms that were brought back to rest now oscillate along y, while the remaining atoms continue to move along the dashed circle. Here, the fraction of atoms brought to rest is small, indicating that both interferometers measure a phase close to π. (b) The standard deviation of the two interferometer outputs σ_+ and σ_- are plotted as the interferometer time t_2 is varied. When the interference contrast is high, σ is large because of phase noise from vibrations and other sources. At $t_2 = 107.7$ ms, both interferometers exhibit good contrast. The output of each interferometer alone appears random, but the correlation between the signals reveals the differential phase.

$R = 0.20$ mm, as shown in FIG. 1. The packets can also be imaged in the yz-plane, which is used to ensure overlap in the z direction.

When the Bragg beam and trap parameters are optimised, we observe simultaneous interference for both packet pairs. Each individual interferometer exhibits phase noise, primarily due to vibrations of the mirror used to retro-reflect the x Bragg beam. The appearance of this noise is an indicator that interference is occurring, as shown in FIG. 2(b). The duration of the contrast peaks indicates a coherence length of 10 μm, which agrees with the Thomas–Fermi condensate size for our trap [27].

Our interferometer output signal is $S = N_0/N$, the fraction of atoms brought back to rest. When the two signals S_+ and S_- are plotted against each other, the data fall on an ellipse, with the eccentricity and orientation of the ellipse set by the differential phase [28]. Example data are shown on the left in FIG. 3. We fit such data to an ellipse to extract the phase $\Delta\Phi$, with an accuracy of about 0.2 rad after ten runs of the experiment.

The effective Sagnac area of the interferometer is $4A = 0.50$ mm^2, which implies a phase shift of about 0.1 rad due to the Earth's rotation. The observed phase differs from this, and in fact depends on the trap and alignment parameters. We attribute this to imperfections in the trapping potential. The phase acquired by a packet as it moves through the trap can be calculated as the integral of the action. The resulting contribution to the differential phase from the trap is [29]

$$\Delta\Phi_{\rm trap} = \frac{4mv_B^2}{\hbar} \sum_{i=x,y,z} \frac{\gamma_i}{\omega_i} \sin\omega_i t_2 \cos\omega_i(t_1+t_2), \quad (8)$$

where $\gamma_i = (\hat{\mathbf{k}}_x \cdot \hat{\mathbf{r}}_i)(\hat{\mathbf{k}}_y \cdot \hat{\mathbf{r}}_i)$ is set by the alignment of the x and y Bragg beam wave vectors $\hat{\mathbf{k}}_x$ and $\hat{\mathbf{k}}_y$ to the trap principle axes $\hat{\mathbf{r}}_i$. The phase can be approximated to second order in small terms as

$$\Delta\Phi_{\rm trap} \approx 4kR\left[\frac{\pi}{7}(4\delta t_1 + 9\delta t_2)\,\omega_0\beta + \frac{2\gamma_z}{\kappa}\cos(2\pi\kappa)\cos\left(\frac{5\pi\kappa}{2}\right)\right], \quad (9)$$

where k is the Bragg wave number, R is the orbit radius, δt_1 and δt_2 are timing errors in t_1 and t_2, β is the xy term in the potential energy as in (7), and $\kappa = \omega_z/\omega_0$. We have verified the predicted dependence on the timing and β, using data as in FIG. 3. Unfortunately, the y Bragg beam passes through a long, thin vacuum tube on the way to the atoms, making it difficult to adjust in a controlled way to test the γ_z dependence. An improved apparatus design will eliminate this constraint and also allow implementation of a spherically symmetric trap, where $\kappa \approx 1$ and the γ_z contribution is reduced. However, anharmonic terms in the potential can also contribute to the trap phase, and will need to be considered.

In order to test the Sagnac sensitivity of the interferometer, we rotated the optical table on which the apparatus sits. The table floats on air legs that allow a few mm of horizontal motion. We used a motorised translation stage to move one end of the table during the interferometer measurement. With a force of about 10 N, linear speeds up to 0.7 mm/s could be achieved. The table motion was initiated prior to the first Bragg pulse of the interferometer sequence, and it continued at a constant speed throughout the measurement. Results are shown in FIG. 3.

Because the rotation measurements were not made using a dedicated rate table, accurate calibration of the rotation rate is difficult. Applying the Sagnac formula to the data in FIG. 3 indicates a rotation calibration v/Ω of 0.5 m, in reasonable agreement with a mechanical estimate of about 1 m. The one-sigma error bars on the plot then correspond to a rotation sensitivity of 8×10^{-5} rad/s, comparable to the rotation rate of the Earth, $\Omega_E = 7.3 \times 10^{-5}$ rad/s. To avoid systematic errors caused by tilting, we ensured that the table remained level to about 50 μrad. For our measured tilt sensitivity, this corresponds to only about 0.03 rad of differential phase.

In summary, we have demonstrated a trapped-atom Sagnac sensor with the largest enclosed area to date and, for the first time, simultaneous counter-rotating interferometers to obtain common-mode noise rejection. We

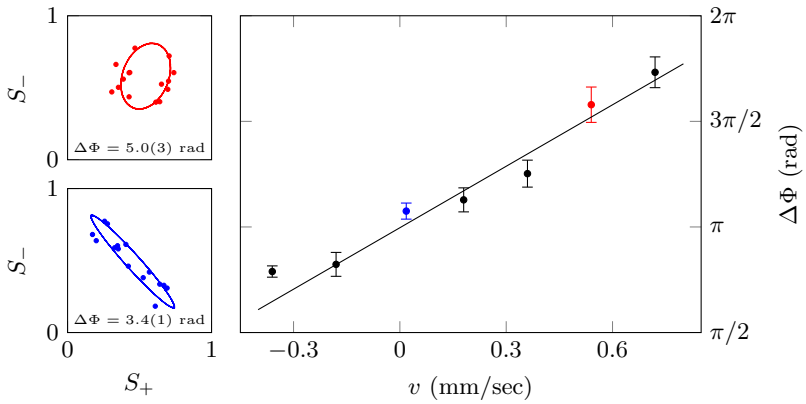


FIG. 3: Left: Points correspond to the two interferometer output signals S_+ and S_- from a given measurement. Curves are ellipses fitted to the points. The orientation and eccentricity of the ellipse reveals the differential phase $\Delta\Phi$ between the interferometers. Right: Dependence of the differential phase on the experimental rotation velocity of the system v, illustrating the Sagnac effect. The offset at $v = 0$ mm/s indicates the trap is not perfectly symmetric. The coloured points correspond to the matching data on the left.

achieve rotation sensitivity comparable to Earth rate, and the residual phase dependence on the trap parameters is described by a simple model.

A number of improvements to the interferometer can be envisioned. The enclosed area can be increased by reducing the trap frequency. The sensitivity grows as the square of the orbit radius R, while the alignment and trap tolerances shrink as only $1/R$. The atoms can also make multiple orbits in the trap, with the sensitivity increasing as the orbit number. The trap tolerances then either remain constant or decrease as the inverse of the orbit number. Using these techniques, we estimate that it is feasible to reach a sensitivity on the order of 10^{-7} (rad/s)/$\sqrt{\text{Hz}}$, which would be attractive for inertial navigation applications. It is also feasible to reduce the size, weight and power of the condensate apparatus to a value comparable to that of existing navigation systems [30]. Through such improvements, we hope to develop this approach into a useful device for rotation sensing applications.

This work was supported by the National Science Foundation and NASA.

* Now at: NASA Langley Research Center, Revolutionary Aviation Technologies Branch, Hampton, Virginia, USA
† Now at: Prince of Songhkla University, Interdisciplinary Graduate School of Earth System Science and Andaman Natural Disaster Management, Kathu, Phuket, Thailand
‡ Email: cas8m@virginia.edu

[1] D. Titterton and J. L. Weston, *Strapdown Inertial Navigation Technology*, 2nd ed. (Institution of Engineering and Technology, London, 2004).
[2] I. P. Prikhodko, S. A. Zotov, A. A. Trusov, and A. M. Shkel, J. Microelectromech. Syst. **22**, 1257 (2013).
[3] G. E. Stedman, Rep. Prog. Phys. **60**, 615 (1997).
[4] M. Cerdonio, G. A. Prodi, and S. Vitale, Gen. Rel. Grav. **13**, 185 (1988).
[5] G. Sagnac, C. R. Acad. Sci. **95**, 708 (1913).
[6] H. C. Lefèvre, *The Fiber-Optic Gyroscope*, 2nd ed. (Artech House, Norwood, MA, 2014).
[7] T. L. Gustavson, A. Landragin, and M. A. Kasevich, Class. Quantum Grav. **17**, 2385 (2000).
[8] D. S. Durfee, Y. K. Shaham, and M. A. Kasevich, Phys. Rev. Lett. **97**, 240801 (2006).
[9] D. Savoie, M. Altorio, B. Fang, L. A. Sidorenkov, R. Geiger, and A. Landragin, Sci. Adv. **4** (2018).
[10] W. Ketterle and D. E. Pritchard, Appl. Phys. B **54**, 403 (1992).
[11] J. A. Sauer, M. D. Barrett, and M. S. Chapman, Phys. Rev. Lett. **87**, 270401 (2001).
[12] A. S. Arnold, J. Phys. B: At. Mol. Opt. Phys. **37**, L29 (2004).
[13] M. Horikoshi and K. Nakagawa, Phys. Rev. Lett. **99**, 180401 (2007).
[14] G.-B. Jo, Y. Shin, S. Will, T. A. Pasquini, M. Saba, W. Ketterle, D. E. Pritchard, M. Vengalattore, and M. Prentiss, Phys. Rev. Lett. **98**, 030407 (2007).
[15] S. Wu, E. Su, and M. Prentiss, Phys. Rev. Lett. **99**, 173201 (2007).
[16] J. H. T. Burke and C. A. Sackett, Phys. Rev. A **80**, 061603(R) (2009).
[17] L. Qi, H. Zhaohui, T. Valenzuela, Y. Zhang, Y. Zhai, W. Quan, N. Waltham, and J. Fang, App. Phys. Lett. **110**, 153502 (2017).
[18] M. Boshier, private communication (2019).
[19] S. Wu, W. Rooijakkers, P. Striehl, and M. Prentiss, Phys. Rev. A **70**, 013409 (2004).
[20] D. M. Giltner, R. W. McGowan, and S. A. Lee, Phys. Rev. A **52**, 3966 (1995).
[21] S. Wu, Y. Wang, Q. Diot, and M. Prentiss, Phys. Rev. A **71**, 043602 (2005).
[22] K. J. Hughes, B. Deissler, J. H. T. Burke, and C. A. Sackett, Phys. Rev. A **76**, 035601 (2007).
[23] Y. J. Wang, D. Z. Anderson, V. M. Bright, E. A. Cornell, Q. Diot, T. Kishimoto, M. Prentiss, R. A. Saravanan,

S. R. Segal, and S. Wu, Phys. Rev. Lett. **94**, 090405 (2005).
[24] O. Garcia, B. Deissler, K. J. Hughes, J. M. Reeves, and C. A. Sackett, Phys. Rev. A **74**, 031601(R) (2006).
[25] R. A. Horne and C. A. Sackett, Rev. Sci. Instrum. **88**, 013102 (2017).
[26] W. Petrich, M. H. Anderson, J. R. Ensher, and E. A. Cornell, Phys. Rev. Lett. **74**, 3352 (1995).
[27] F. Dalfovo, S. Giorgini, L. Pitaevskii, and S. Stringari, Rev. Mod. Phys. **71**, 463 (1999).
[28] G. T. Foster, J. B. Fixler, J. M. McGuirk, and M. A. Kasevich, Opt. Lett. **27**, 951 (2002).
[29] E. Moan, Z. Luo, and C. A. Sackett, in *Proc. SPIE 10934, Optical, Opto-Atomic, and Entanglement-Enhanced Precision Metrology, 109341X* (IEEE, New York, 2019) p. 10.1117/12.2515457.
[30] D. M. Farkas, K. M. Hudek, E. A. Salim, S. R. Segal, M. B. Squires, and D. Z. Anderson, Appl. Phys. Lett. **9**, 093102 (2010).